ELSEVIER

Journal of Chromatography A, 945 (2002) 117–131

JOURNAL OF CHROMATOGRAPHY A

www.elsevier.com/locate/chroma

Study of feed temperature control of chromatography using computional fluid dynamics simulation

C.B. Ching[a,*], Y.X. Wu[a], M. Lisso[b], G. Wozny[b], T. Laiblin[c], W. Arlt[c]

[a]*Department of Chemical and Environmental Engineering, National University of Singapore, Singapore, 119260, Singapore*
[b]*Institute of Process and Plant Design, Department of Dynamics and Processes of Technical Plants, Sekr. KWT 9, Technology University of Berlin, Strasse des 17. Juni 135, 10623 Berlin, Germany*
[c]*Institute of Chemical Engineering, Department of Thermodynamics and Thermal Chemical Engineering, Gebäude TK 7, Technology University of Berlin, Strasse des 17. Juni 135, 10623 Berlin, Germany*

Received 26 March 2001; received in revised form 25 September 2001; accepted 6 November 2001

Abstract

Recently preparative high-performance liquid chromatography (HPLC) has been used more and more frequently to separate drugs and natural substances. However, large-scale HPLC easily tends to reduce the yield and purity of the product. Hydrodynamic and heat factors play an important roles. Generally, in a large-scale HPLC column, the tracer profile inside column will take on a parabolic shape because of the distributor, which will impact the separation performance of the column. With the inlet temperature suitably lower than the wall temperature, this situation could be improved to some extent. In this work, some experiments were conducted using HPLC, with a column 10 cm in diameter to determine the optimal temperature difference between wall and inlet temperatures. The wall temperature was fixed at about 30 °C and the inlet temperature varied from 15 to 30 °C. The flow-rate of the eluent, methanol, was 300 ml/min. The experimental result was simulated using CFD software FLUENT 4.4.4. The simulated temperature field fitted the experimental one very well and the simulated flow, temperature and tracer distribution inside column could provide good explanation of separation performance under different conditions. In addition, the simulation could at least approximately predict the optimal temperature difference. © 2002 Elsevier Science B.V. All rights reserved.

Keywords: Temperature control; Simulation; Computational fluid dynamics; Preparative chromatography; FLUENT

1. Introduction

With the development of chemical and biochemical industries, HPLC on a large scale has become more and more important. However, it is often found that the separation performance of preparative chromatography declined after scale-up. To promote the separation efficiency of preparative chromatography, we need to properly understand the controlling effects of the process, which may enable us to predict the process and to improve the design and operation of preparative chromatography. Therefore, the research of hydrodynamic factors and heat effects pertaining to the separation performance of large-scale chromatography becomes very important. In the review of Lode and Rosenfeld, et al. [1], improper column packing, poor distributors and dispersion in auxiliary apparatus were factors that

*Corresponding author. Fax: +65-8-731-994.
E-mail addresses: cpehead@nus.edu.sg (C.B. Ching), engp8896@nus.edu.sg (Y.X. Wu).

0021-9673/02/$ – see front matter © 2002 Elsevier Science B.V. All rights reserved.
PII: S0021-9673(01)01479-0

impaired the separation performance of large-scale chromatography. The packing quality and its effect on the performance of HPLC have also been investigated in detail [2–7]. Arlt et al. [8] examined the effect of the frit with the aid of the CFD software FLUENT. Their study showed that the quality of the distributor greatly affects the performance of large-scale chromatography.

Besides the physical factors such as the packing quality and the distributor, temperature also plays a very important role in the chromatographic process. A lot of work has been devoted to examining the influence of temperature on the thermodynamics and kinetics of the separation process in chromatographic columns [9–14]. Ooms [15] summarized the increasing role of temperature control in LC by examining some typical applications to illustrate its present use and future potential. Dapremont et al. [16] pointed out that: (1) because the heat transfer in the packed bed is quite slow, a radial temperature gradient will exist in the column and this reduces the column efficiency. (2) The performance of a large-diameter chromatographic column could be drastically affected when the solvent enters the column at a temperature different from that of the wall of column. (3) The effect of the temperature difference between the inlet and the wall of the column is closely related to the flow-rate, as well as the length and the diameter of the column. Thus it is necessary to control both the temperatures of the mobile phase and the column wall to ensure good reproducibility and good column performance. To some extent the work of Brandt, Mann and co-workers [17,18] confirmed these conclusions. They analyzed the strong effect of dissipation of viscous heat, as well as the distributors and the collectors on the performance of HPLC, and found that with a suitable lower eluent temperature the poor performance of a large-scale chromatographic column may be improved. In addition, they visualized their results using a transparent glass column and some dye tracers.

Although these studies showed the effect of the radial temperature gradient on the performance of a chromatographic column, they do not thoroughly explain these phenomena. To this end, computational fluid dynamics (CFD) should be very helpful. CFD simulation involves the numerical solution of conservation equations for mass, momentum and energy in a flow geometry of interest, together with additional sets of equations reflecting the problem at hand. CFD has long been known as an aid in the engineering of fluid flow systems. However, its potential was only realized and it became of interest to the chemical engineer in the last decades. Colenbrande [19] has prepared a review on CFD applications in the petrochemical industries with specific emphasis on CFD applications and the related experimental work carried out in the Shell Group laboratories. Harris et al. [20] have presented a review on the application of CFD in chemical reaction engineering with emphasis on single-phase flow applications. In addition, Kuipers and van Swaaij [21] have systematically reviewed the application of CFD to chemical reaction engineering. Also, for columns of different sizes and different operation conditions, such as flow-rate and chemicals, a lot of experiments must be done to determine the optimal temperature difference between the inlet and the wall of the column. If helpful predictions are available, a lot of time, financial and manpower resources can be saved.

Therefore, the purposes of this study were twofold. The first one was to find the optimal temperature difference between the inlet and the wall of the column under some fixed conditions by means of experiments and CFD simulations. Through matching the simulation result with experimental result, the CFD simulation to the chromatographic process will be validated at the same time. The second purpose of this study was to achieve a better understanding of the hydrodynamic phenomena occurring during the chromatographic process so as to understand the mechanism of temperature control.

2. Experiment

2.1. Chemicals

Solid phase: silica gel with diameter range 40–60 μm (Ueticon, Germany). Solvent: methanol of 99.8% in purity (Merck, Germany). Tracer: toluene of 99.8% in purity (Aldrich, Germany).

2.2. Set-up

A schematic graph of the experimental apparatus is shown in Fig. 1. Methanol was pumped into the

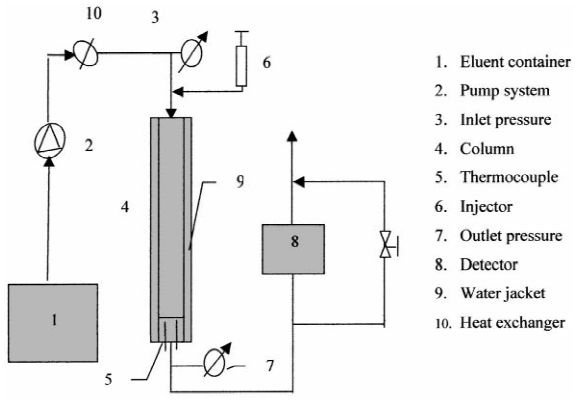

Fig. 1. Experimental set-up.

heat exchanger, where it was heated to the inlet temperature. It passed by the determining points of the inlet pressure and the inlet temperature, and entered the HPLC column (10 cm, I.D.) Merck (Germany), which was packed with a normal-phase silica gel (Ueticon). The fixed bed was 38 cm in length. Frits of 5 mm thick were implemented at both ends of the column. The wall of the column was thermostated at 30 °C by means of a water jacket fed by a temperature bath (Haake, Germany). The water jacket was wrapped with insulation material. Then Pt100 thermocouples were implemented into the end of the column, positioned at 5 cm in front of the outlet over the column radius, to determine the radial temperature distribution. The samples were detected using a UV detection system. A PC equipped with the measurement software FLEXPRO-CONTROL was used to register temperatures (inlet, wall, outlet, and radial distribution), pressures (inlet and outlet), and to detect signals online. After passing the detection system, the eluent was either recycled to the eluent container or discharged into the waste container if contaminated by the tracer.

The tracer was injected into the system using a six-port injection valve with a 5-ml sample loop after the system reached thermal equilibrium. The flow-rate was kept at 300 ml/min and the wall temperature was 30 °C. The eluent temperature at the inlet was varied to 15, 20, 25 and 30 °C. The fluctuation range was <0.1 °C. For each set of operation conditions, the measurement was repeated at least three times for reproducibility. It generally took 0.5 h to reach steady status between repeated measurements and 1 h between different operating conditions.

2.3. Determination of porosity

The weighting method was applied to measure the total porosity. The measurement was conducted at 25 °C. A small column ($Ø=10$ mm and $L = 25$ cm) was chosen for the measurement. The weight of the empty column was measured first as W_c. Then, the weight of the column full of the solid packing particles was measured as W_{cs}. The next step was to pack the column with slurry—the mixture of the solid particles and four solvents, methanol (0.79 g/ml), water (0.997 g/ml), isopropanol (0.781 g/ml) and chloroform (1.474 g/ml). The total weights after packing were W_{csf1}, W_{csf2}, W_{csf3} and W_{csf4}, respectively. The total weight vs. density of solvent was plotted and the slope gave the volume of the fluid in the packed column, which was found to be 16.059 cm^3. The volume of the column was 19.63495 cm^3. Therefore, the total porosity is 0.818, the ratio of the fluid volume to the column volume.

The internal porosity measured in this study is the ratio of the internal pore volume to the volume of the column. A certain amount of the solid packing particles was put into a beaker containing a stirrer. Then isopropanol was dropped from a vertically installed burette into the beaker. Dry solid packing particles will adsorb isopropanol into its internal pores for the capillarity. Before the saturation point, the solid particles in the beaker remained unchanged. When all the internal pores were full of the solvent, if a little more solvent was added, the solvent would spill out to the surface of the particles, making the particles stick to one another. At this point, one could observe that the solid particles ‘exploded’ to fill the whole beaker. The volume of isopropanol consumed from the beginning to this point was equal to the volume of the internal pores. Therefore, the internal porosity was the ratio of the volume of the consumed isopropanol to the column volume, which was found to be 0.34.

2.4. Data analysis method

The method of moments [22] was used to calculate the retention time and the height equivalent to a theoretical plate (HETP)

$$\text{The first moment: } \mu = \frac{\int_0^t ct\,\mathrm{d}t}{\int_0^t c\,\mathrm{d}t} \quad (1)$$

$$\text{The second moment: } \sigma^2 = \frac{\int_0^t c(t-\mu)^2\,\mathrm{d}t}{\int_0^t c\,\mathrm{d}t} \quad (2)$$

$$\text{Number of theoretical units (NTU): NTU} = \frac{\mu^2}{\sigma^2} \quad (3)$$

$$\text{HETP} = \frac{L}{\text{NTU}} \quad (4)$$

where L is the length of the fixed bed.

3. Results and discussions

Fig. 2 illustrates the radial temperature distribution at the surface of 5 cm before the column outlet. The temperature gradient near the wall is quite sharp. However, near the center of the column, the curve is pretty flat. The value is a little higher than the inlet temperature. This temperature elevation probably comes from two causes: one is the radial heat transport and the other one should be the viscous heat produced by the pressure drop along the column.

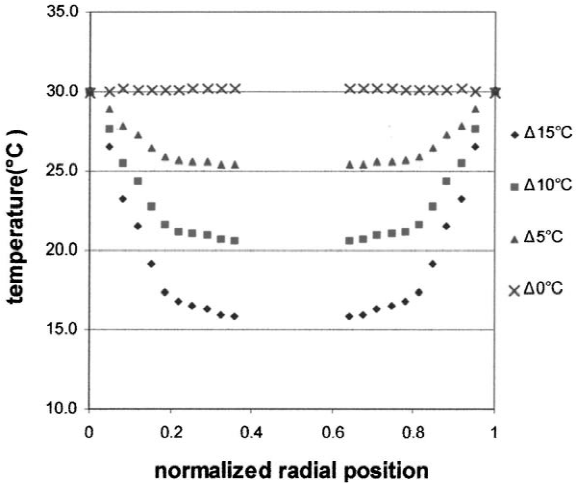

Fig. 2. Radial temperature distribution, at 5 cm before the column outlet under different inlet temperatures and T_{wall} of 30 °C with a flow-rate of 300 ml/min.

$$\mathrm{d}Q = \mathrm{d}U + V\,\mathrm{d}P + P\,\mathrm{d}V \quad (5)$$

In this study, dU and dV are 0, so

$$\mathrm{d}Q = C_\mathrm{p}\,\mathrm{d}T = V\,\mathrm{d}P \quad (6)$$

where V is constant. The density and the heat capacity can be considered to be constant over a small temperature range. Thus

$$\Delta T = \frac{V\,\Delta P}{C_\mathrm{p}} = \frac{\Delta P}{\rho C_\mathrm{p}} \quad (7)$$

The pressure drop was around 5 bar. The column radius was 0.05 m and the length from the inlet to the radial temperature-determining surface was about 0.33 m. The density was 786 kg/m^3 and the heat capacity C_p was 2534 J/(kg K). Thus the increase of temperature due to the pressure drop should be around 0.22 K. This may explain the temperature elevation in the central part of the column, which is 30 °C at the inlet. For each experiment, this value should only show a small difference due to the fluctuation of the pressure drop and the slightly varied density as well as the heat capacity. However, the temperature elevation became more and more with the increment of the temperature difference. One main reason should be the experimental device and the experimental environment. The position where the inlet temperature was determined was about 20 cm away from the actual inlet of the column and the temperature of the surrounding environment was about 25 °C. For the experiment with eluent temperature of 15 °C at the inlet, although the 'inlet temperature' was shown on computer as 15 °C, the environment to some extent would heat up the eluent; hence its temperature in the central part was elevated more than that of the experiment with inlet temperature of 30 °C. Accordingly, the temperature elevation of experiment with the inlet temperature of 20 °C was in between.

The eluted pulse responses are shown in Fig. 3. Several phenomena can be observed from the graph. First, the peak position decreases with the increase of the inlet temperature. Probably this is partly because a slight adsorption occurred. The influence of temperature on retention time is a function of the free

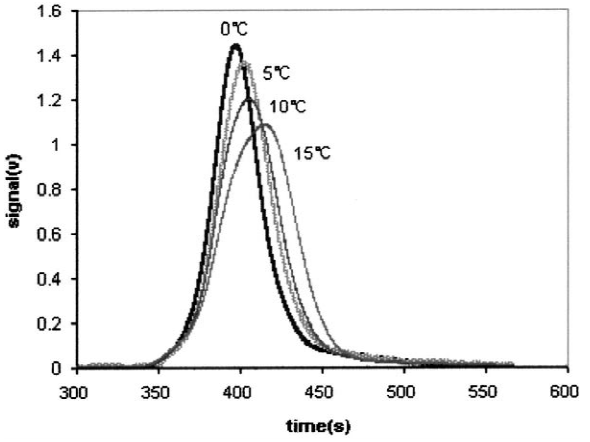

Fig. 3. Eluted responses with different temperature differences.

energy changes in the interaction between the analyte and the stationary phase. In common normal- and reversed-phase separations, retention reactions are usually exothermic with relatively small enthalpy changes that cause modest decreases in retention times when the temperature increases [15]. In this study, the adsorption effect of toluene on the normal-phase silica gel using methanol is very small. The temperature influence is still smaller because methanol is much more polar than toluene and effectively suppresses the adsorption of toluene. Thus, the effect of temperature on retention time and peak position is very small. The shift of peak position is also partly due to the deformation of the eluted pulse. For example, when the eluent temperature was 15 °C, the eluted pulse shows obvious fronting, resulting in the delayed peak position, but the retention time should be a little before the peak position due to the fronting. Secondly, the height of the peak decreases with the inlet temperature. Generally, the sharper the peak, the better the separation performance. Fig. 3 embodies all of these except that the optimal inlet temperature might be around 25 °C although the breakthrough curve in the case of the inlet at 30 °C looks sharper. The HETP shown in Fig. 14 verifies this result. Comparing the curves of the two cases carefully, it can be found that the tailing of inlet 30 °C is serious. After 460 s the concentration of the case at ΔT of 0 °C maintains higher than that at ΔT of 5 °C. It seems that with the inlet temperature 5 °C lower than the wall temperature, the negative effect of the distributor was offset to some extent and thus the column shows better separation capability. The following simulation should provide a clear explanation. On the basis of the experimental and simulation results for these four cases, more detailed work was carried out as described in the following sections.

4. Simulation

In this study the CFD software FLUENT 4.4.4 was used to simulate the experimental result. The CFD software is able to provide detailed information about the velocity, the temperature, as well as the mass distributions within the examined HPLC column. So it enables us to understand how the process develops inside the column in order to recognize the most important factors, and therefore, to achieve improved separations.

4.1. Assumptions

The tracer used was toluene, which was only slightly adsorbed into the normal solid-phase column used in the experiments. We tried to include the adsorption term in the component balance equations using this software but failed to obtain acceptable results. Because this study focused on the hydrodynamics in the column, we assumed that there was no adsorption occurring. The column diameter was 10 cm, and the ratio of column diameter to particle diameter was about 2000, therefore it was assumed that there was no wall effect and that the column was homogeneously packed. The axial symmetric distribution of physical properties was also assumed. Dissipation caused by viscous heat was assumed to be negligible.

4.2. Theory

The momentum model for porous media used in FLUENT was the Navier–Stokes equation modified by Darcy's Law:

$$\frac{\partial P}{\partial x_i} = -\frac{\eta}{\alpha_i} v_i \tag{8}$$

where i refers to coordinate r or z.

Vortmeyer's pseudohomogeneous mathematical

model [23] for a packed bed was applied in the simulation for the energy balance. In this convection–dispersion model, the temperatures of the solid phase and the liquid phase were assumed to be the same.

$$\frac{\partial}{\partial t}\left[\epsilon\rho_f c_{pf}T + (1-\epsilon)\rho_s c_{ps}T\right] + \frac{\partial}{\partial z}(\rho_f v_z c_{pf}T) + \frac{\partial}{\partial r}(\rho_f v_r c_{pf}T) = \frac{\partial}{\partial z}\left(\lambda_{eff}\frac{\partial T}{\partial z}\right) + \frac{1}{r}\frac{\partial}{\partial r}\left(\lambda_{eff} r \cdot \frac{\partial T}{\partial r}\right) \quad (9)$$

The component balance was also a convection–dispersion model as follows:

$$\frac{\partial c}{\partial t} + v_z\frac{\partial c}{\partial z} + v_r\frac{\partial c}{\partial r} = D_{ax}\frac{\partial^2 c}{\partial z^2} + \frac{1}{r}\frac{\partial}{\partial r}\left(D_{rad} r \cdot \frac{\partial c}{\partial r}\right) \quad (10)$$

In simulation, the dispersion coefficients were assumed to be independent of the composition of the fluid phase since the solution is quite dilute in the column.

4.3. Simulation set-up

The structure of the simulated column is illustrated in Fig. 4. The geometry is divided into five segments in the axial direction and two segments in the radial direction. Axially the five segments from left to right are the inlet, the distributor, the fixed bed, the collector and the outlet. The dashed line, which is 33 cm away from the inlet, is the face where the radial temperature distribution is measured. In the radial direction, the border between the two segments is the radius of inlet and outlet. Since the column is axially symmetric, it is enough to simulate only half of the column.

In the simulation, the grid density was about ten cells per centimeter. FLUENT 4.4.4 is based on the finite volume method, thus the HETP was related to the grid density due to the numerical dispersion. The variation of the HETP became less and less with the increase of the grid density. When the grid density was up to 10 cells/cm, the variation was very small. If the density continued to increase, the calculation time would expand sharply without much further improvement [24]. In the areas of the distributor and the collector, a higher grid density (20 cells per cm) was allocated because the velocity changes more intensely there. The detailed information is shown in Table 1.

4.4. Simulation parameters

The parameters used in the simulation are listed in Table 2. All units are the same as those used within FLUENT. Constant values of the fluid density and the heat capacity were used because they do not change much in the temperature range of our work. However, this is not true for the viscosity. For example, there is a change of 8.95% in the viscosity between 300 and 295 K ($\eta = 7.4 \cdot 10^{-4}$ kg/(m s) and $\eta = 8.062 \cdot 10^{-4}$ kg/m s)! In addition, the velocity is

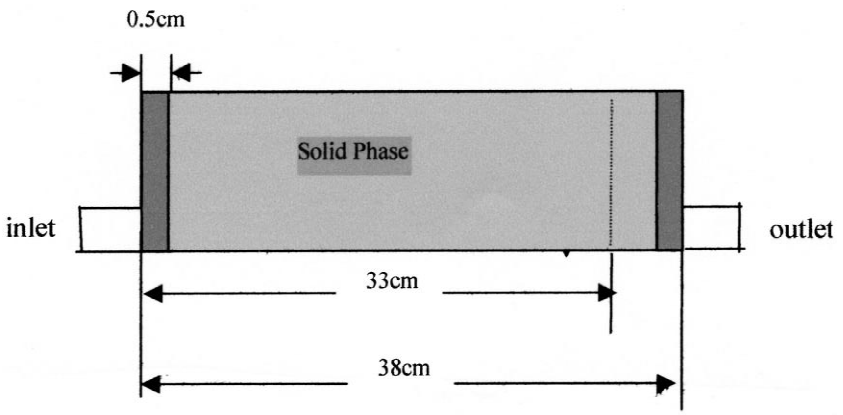

Fig. 4. Structure of simulation geometry.

Table 1
Grid distribution

Segment	Axial direction					Radial direction	
	Inlet	Distributor	Fixed bed	Collector	Outlet	Inlet	Bed-inlet
Size (cm)	1	0.5	37	0.5	1	0.7232	4.2768
No. of cells	10	10	360	10	10	7	43

strongly affected by the viscosity. Therefore the viscosity was implemented as a function of temperature for all simulations with an energy balance included. The effective heat conductivity was used in the simulation. In FLUENT [25]

$$\lambda_{\text{eff}} = \epsilon_t \lambda_f + (1 - \epsilon_t)\lambda_s \quad (11)$$

where ϵ_t is the total porosity. The effective value for the heat conductivity of the packed bed filled with methanol was measured experimentally and found to be 0.323 W/(m K) and 0.338 W/(m K) at 20 and 40 °C, respectively. It was measured after the mixture of eluent and solid phase had settled down, thereby, the values were static. In the experiment, owing to the influence of the fluid flow, the dynamic value should be larger than the static value; hence in simulation we changed the effective heat conductivity until the simulated temperature curve matched the experimental results. In this way, the value of 0.5 W/(m K) was obtained, which was higher than the static value.

One of the parameters of porous media, the frit quality (FQ), may be unknown to most people. It was defined by Lisso et al. [26]. For porous media, the Navier–Stokes equation (NSE) is extended with Darcy's law:

$$\frac{\partial P}{\partial z} = -\frac{\eta}{\alpha_z} v_z \quad \frac{\partial P}{\partial r} = -\frac{\eta}{\alpha_r} v_r \quad (8')$$

The Darcy's term in NSE becomes dominant because of the low values of the axial and radial permeability α_z and α_r. The dimensionless analysis leads to the dimensionless number FQ which is the ratio of the axial and radial pressure loss gradient under the assumption of the same axial and radial

Table 2
Experimental and simulation parameters

Part	Parameter	Parameter value
Fluid phase	Density ρ	786 kg/m^3 For momentum balance only $\eta = 7.4 \cdot 10^{-4}$ kg/(m s)
	Viscosity η	For simulation with energy balance [27] $\eta = -1.6105031 \cdot 10^{-9} T^3 + 1.6029168 \cdot 10^{-6} T^2 - 5.39343878 \cdot 10^{-4} T + 6.17642570 \cdot 10^{-2}$ kg/(m s)
	Heat capacity	$C_p = 2534.2$ J/kg K
	Thermal conductivity $\lambda_f = \lambda_{\text{eff}}$	0.5 W/(m K) (validated by simulation)
Solid phase	Heat capacity	$C_p = 1000$ J/kg K
	Density	$\rho_s = 2400$ kg/m^3
	Total porosity ϵ_t	0.818
	External porosity ϵ	0.478
	Permeability	$\alpha_{\text{axial-bed}} = 1.10 \cdot 10^{-12}$ m^2 $\alpha_{\text{axial-frit}} = 1.10 \cdot 10^{-13}$ m^2 $\alpha_{\text{radial-frit}} = 1.10 \cdot 10^{-11}$ m^2 (FQ=100) $\alpha_{\text{radial-frit}} = 5.50 \cdot 10^{-12}$ m^2 (FQ=50)
Operation	Velocity in column v_c	$1.3318 \cdot 10^{-3}$ m/s
	Inlet velocity	$6.3662 \cdot 10^{-2}$ m/s

velocities, as shown in Eqs. (12) and (13). Hence the dimensionless number FQ is a possible way to characterize the hydrodynamic distribution behavior of a frit.

$$\frac{\partial P/\partial z}{\partial P/\partial r} = \frac{\frac{\eta}{\alpha_z}v_z}{\frac{\eta}{\alpha_r}v_r} = \mathrm{FQ}\cdot\frac{v_z}{v_r} \tag{12}$$

$$\mathrm{FQ} = \left.\frac{\partial P/\partial z}{\partial P/\partial r}\right|_{v_z=v_r} = \frac{\alpha_r}{\alpha_z} \tag{13}$$

The value of FQ can be easily determined by experiments. Lisso et al. [26] measured the axial and radial pressure loss of a common metal frit and a sintered frit at different volume flows and radial positions from the values of α_z and α_r. The FQ was found to be 47 for a sintered frit and 98 for a metal frit. Therefore, in this study the values of 50 and 100 were put into simulation, respectively and the corresponding simulated result would be compared with experiment. It was assumed that in a fixed bed the radial and the axial permeability were the same due to the homogeneous packing and that they should be ten times as large as the frit axial permeability.

4.5. Boundary conditions

The no-slip boundary was used for the momentum balance, which means velocity drops to zero at column wall. For energy balance, $\partial T/\partial z = 0$ was set for both end-walls, which means no heat flux through the wall at both ends. $T|_{\mathrm{wall}}$ and $T|_{\mathrm{inlet}}$ depended on the particular case.

4.6. Simulation procedures

The simulation was carried out step by step. At first only the momentum balance was solved. The validation of velocity was performed after the stationary solution was reached. Then the energy balance model was activated. Here the viscosity was set as a polynomial function of temperature. The velocity and the temperature fields were checked and compared with the experimental results. If the simulated results matched well with the experiment, the time-dependent model was switched on with time step 0.1 s. At first the mass fraction of species 1 at the inlet was set to 1. After one time step, it was set to 0 again. At last the velocity, temperature and tracer profiles within the column were plotted using the postprocessing tools. The user-defined subroutines were composed and integrated with the software to collect the data of the eluted pulse.

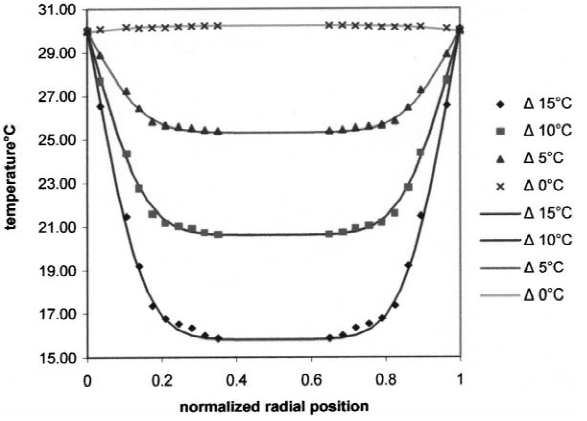

Fig. 5. Validation of the radial temperature distribution at FQ50.

4.7. Results and discussion

4.7.1. Temperature distribution

Figs. 5 and 6 display the comparison between the experimental results and the simulated radial temperature distributions at 5 cm before exit under two different values of FQ. The simulated results fit the

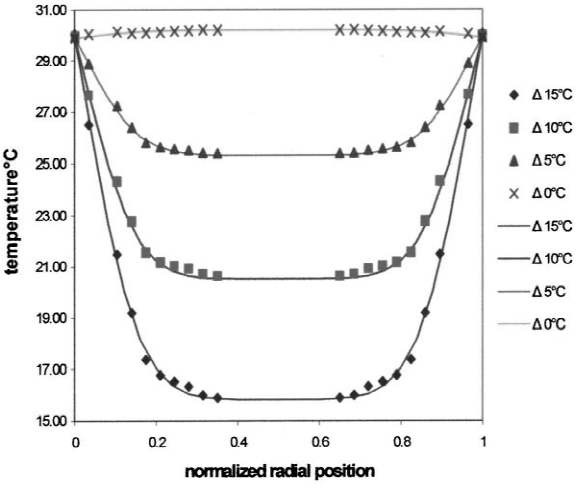

Fig. 6. Validation of the radial temperature distribution at FQ100.

experimental results very well, and that the frit quality FQ has nearly no influence on the temperature profiles.

4.7.2. Functions of frit

The velocity contour and velocity vector are illustrated in Figs. 7 and 8. The velocity only varies much at the area close to the frits. Fig. 8 only shows a small part of the column. The dashed line refers to the column axis. The length of the vectors represents the magnitude of velocity. The radial permeability in the frit is higher than the axial permeability so that the fluid meets less resistance in the radial direction. Therefore, in the frit, the horizontal fraction of the velocity, u, is larger than the vertical fraction, v, in the lower radial position. The horizontal fraction decreases with increasing radial position. In the higher radial position in the frit (near sidewall of the column), the value of v becomes dominant and the u becomes very small. In this way, the frit accomplishes a complete distribution of the fluid over the column diameter soon after the fluid enters into the column. However, because u is larger near column center than that near sidewall, the tracer molecules near center will go farther than those near sidewall. This results in the curvature of tracer profile, which will impair the separation capability of the column. Improving FQ can reduce the curvature, which will be shown in the next section.

4.7.3. Tracer profiles within the column

Fig. 9 illustrates the tracer profiles in column. There are two groups: the frit quality FQ of the left group is 50 and the right is 100. From the two groups the axial dispersion can be observed: the width of the profile is growing while tracer is proceeding downstream. The extent of dispersion near the sidewall is the same as that in the column center. At 10 s, the tracer profile just after the frit with FQ50 shows larger curvature than the group with FQ100, just as what mentioned in the last section. Hence, to increase FQ is a way to improve the performance of a column, but the improvement would cease after the FQ reaches a critical value [8].

When the wall and the eluent are kept at the same temperature, the shape of the tracer profile does not change with time, as illustrated in Fig. 9d and h. This is because of the homogeneous packing. The flow reaches steady status similar to plug flow after a transition zone near frit, as shown in Figs. 7 and 8.

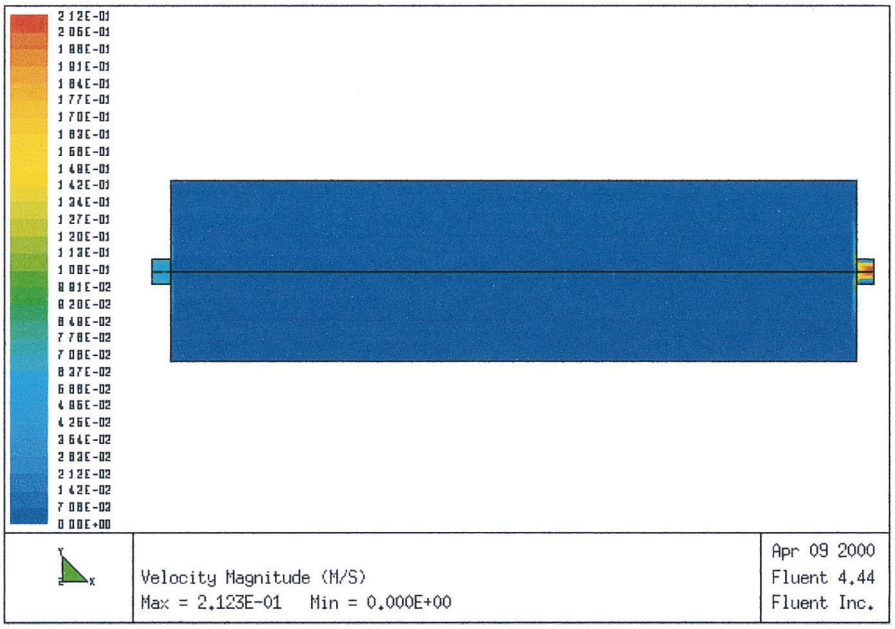

Fig. 7. Velocity contour under a flow-rate of 300 ml/min.

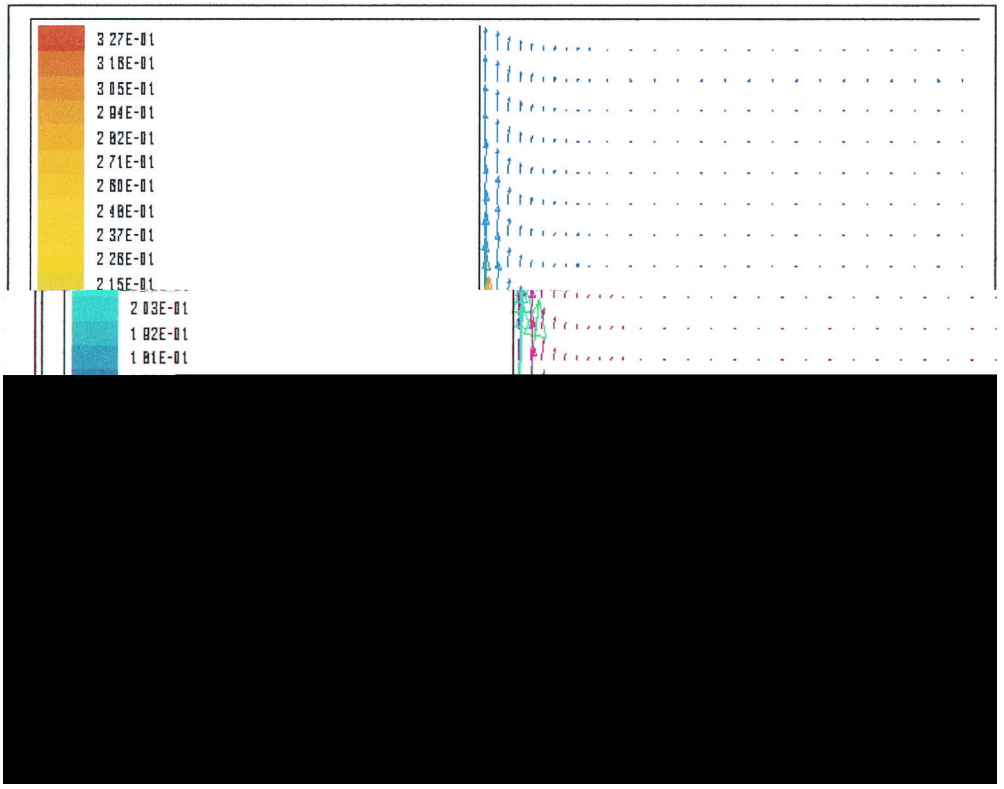

Fig. 8. Velocity vector under a flow-rate of 300 ml/min.

The steady 'plug flow' keeps the shape of tracer profile.

When the eluent temperature is lower than the wall temperature, the fluid near wall is warmed up by the wall and thus its viscosity decreases, so it flows faster than the fluid near center, resulting the reversed tracer shape. Therefore, when the temperature difference is not zero, the shape of tracer profiles distorts while tracer flows forward. When the temperature difference is small, the core of the profile reaches the outlet first, which might results in peak tailing of the eluted pulse. This situation can be observed in Fig. 9d and h. When the temperature difference increases to some extent, the edge of the profile will reach the outlet first instead, as illustrated in Fig. 9a–c and e–g; this will result in peak fronting. Both peak tailing and peak fronting will harm the separation result. The simulated tracer profiles in Fig. 9 can be compared with the experimentally observed profiles shown in Fig. 10, which is from literature [18].

Although FQ shows no effect on the temperature distribution, it greatly influences the function of the frit, the tracer profile inside the column and thus the separation performance of the column. Fig. 9 illustrates the difference between the two groups of FQ50 and FQ100. When FQ is equal to 100, the core of the tracer profile is flatter, which indicates a smaller temperature difference for compensating the effect of distributor. A little larger temperature difference easily causes peak fronting, which will be shown in the next section.

4.7.4. Eluted pulse responses

The simulated pulse responses for columns at FQ50 are shown in Fig. 11 and those at FQ100 in Fig. 12. Both figures show that with a small temperature difference, peak tailing happens; however, when

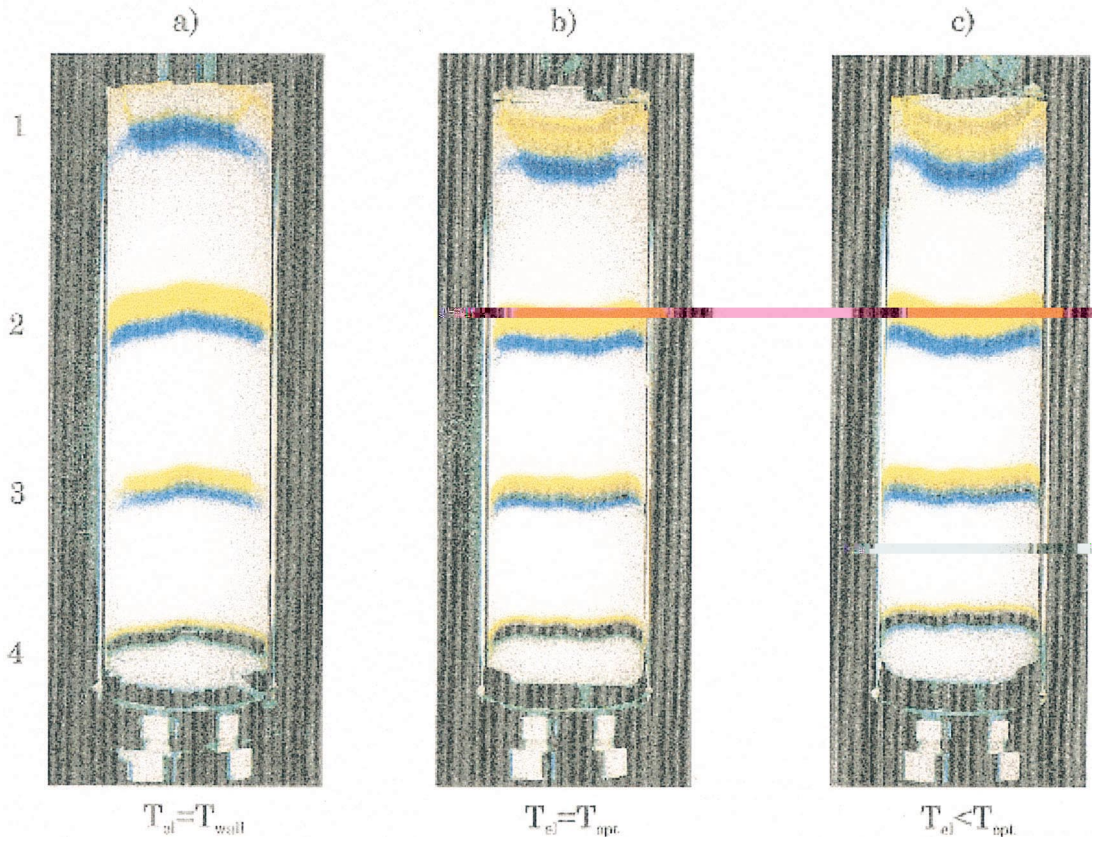

Fig. 10. Photograph of a mixture of three colours eluting from a C_8-RP material with different eluent temperatures, (a) $T_{el}=T_{wall}$; (b) $T_{el}=T_{opt}$; (c) $T_{el}<T_{opt}$ [18].

sponding peak in Fig. 11 when the temperature difference is large; the peak becomes very sharper than the corresponding peak in Fig. 11 when the introduced eluent temperature is suitably lower than the wall temperature.

The two figures show that when the temperature

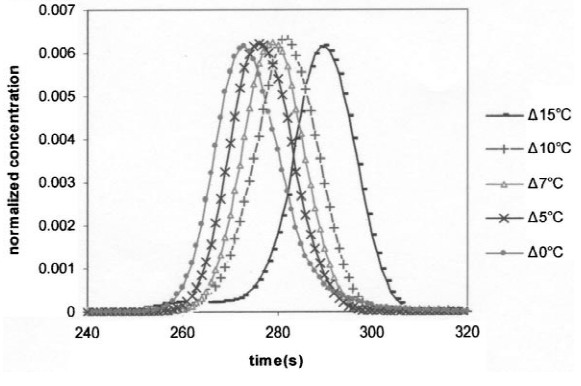

Fig. 11. Simulated pulse response at FQ50.

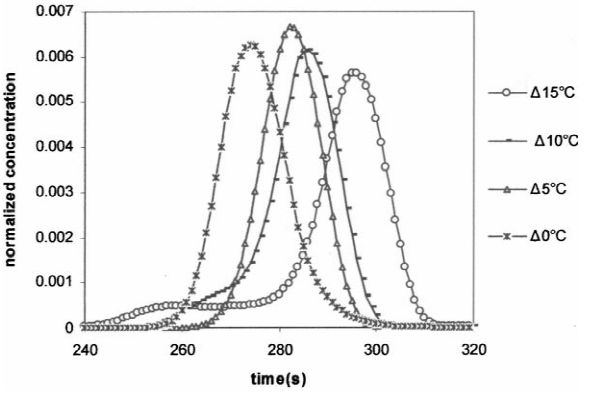

Fig. 12. Simulated pulse response at FQ100.

difference is 5 °C, the eluted pulses are quite symmetric and no peak fronting and tailing are observed, which indicates that the optimal temperature difference should be around 5 °C.

4.7.5. Separation efficiency

The data of the eluted pulse were analyzed using the Method of Moments. HETP, which is the length of the fixed bed over NTU, is plotted in Fig. 13 with respect to the temperature difference ΔT. The variation of HETP with a different ΔT is more sensitive for FQ100. With a large ΔT, the column with a frit of FQ100 operates worse compared to the case of an eluent temperature of 30 °C, while for FQ50 the difference is very small. In addition, among the four experiments, the optimal inlet temperature should be around 25 °C. Therefore more experiments should be carried out around 25 °C to find the exact optimal point, which is in agreement with the experimental observation.

4.8. Optimal temperature difference

From the work described above, the optimal eluent temperature should be around 25 °C. Therefore, the experiments with eluent temperatures 22, 24, 26 and 28 °C were carried out. At the same time, simulations with inlet temperature from 21 to 28 °C were performed, too. The result is shown in Fig. 14. Because of the similar phenomena, the corresponding eluted pulses are not listed here one by one. In order to observe the difference between results of FQ50 and FQ100 more easily, the point at ΔT of 15 °C is not shown. In fact the right branch for FQ100 will rise very high. There was fluctuation of signal when most of the pulse has been eluted during the experiment. In addition, each experimentally determined pulse response shows a small tail. These two facts result that the calculation of HETP for experimental pulse cannot be so easy and accurate as that for simulated pulses. Therefore, in Fig. 14 error bar of 3% is shown for the HETP of experiment.

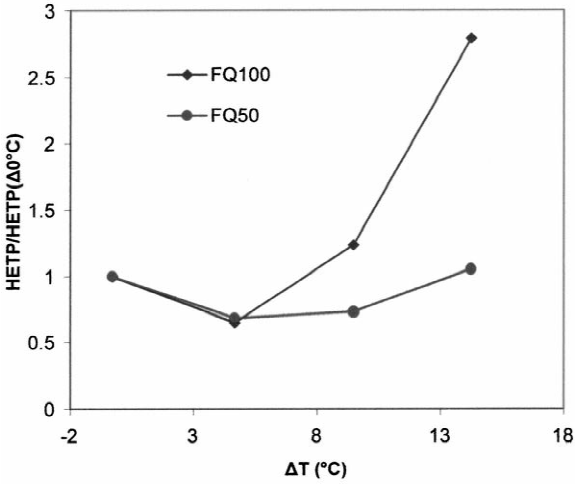

Fig. 13. Simulated variation of HETP.

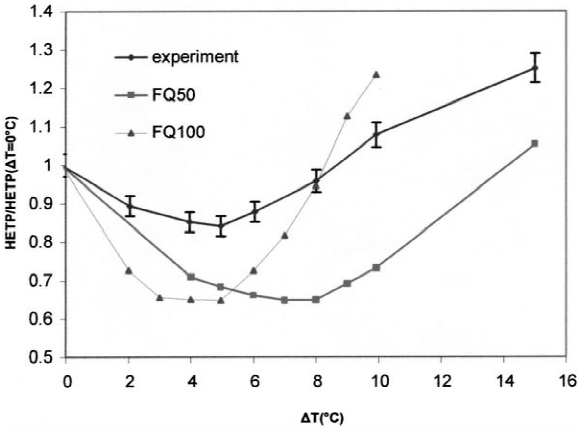

Fig. 14. Optimal ΔT of experiments and simulations at FQ50 and FQ100.

If neglecting the error bar, the experimentally measured optimal temperature difference ΔT is 5 °C, which is consistent with the prediction of simulation with FQ100. The optimal ΔT is 7 °C for FQ50, so the difference between the optimal points of FQ50 and FQ100 is about 2 °C. However, noticing the error bar, the optimal point is probably located in the range of Δ4–Δ6 °C. The prediction of simulation with FQ100 can be seen as in the range of Δ3–Δ5 °C because in this range the HETP is very close to one another although the lowest HETP is shown at Δ5 °C. Obviously the prediction of FQ50 is outside the range predicted by experiment. Therefore, it can be concluded that FQ100 is closer to the real value of FQ and made a better prediction to the experiment than FQ50.

Comparing the simulated and the experimental results shown in Fig. 14, their HETPs differ a lot on

value although they show the similar tendency of variation. The difference in the value of HETP comes largely from the dispersion or diffusion coefficients. The main target of this study is to use temperature difference for reshaping the tracer profiles so as to improve the separation capability of HPLC. Lisso et al. [26] have found that the optimal eluent temperature is independent of dimensionless numbers Re ($du\rho/\eta$) and Bo (uL/D). Therefore, work on the aspects such as the effect of intraparticle diffusion on the peak dispersion is unnecessary. The final result of this work shows that the CFD simulation can qualitatively predict the optimal eluent temperature for the performance of HPLC.

5. Conclusions

It was hypothesized that the frits of bad quality and the temperature gradient inside the chromatographic column could worsen the separation capability of the column and that with different temperatures between the inlet and the wall these negative effects could be counteracted to some extent. The CFD simulation in this study not only confirmed all of these but also provided the detailed information of the stationary velocity, temperature fields and the concentration field at different times. Such information enables us to thoroughly understand the mechanism of these effects. With better frit quality, from the center to the wall, the axial velocity inside the frits will dominate later so as to achieve a more homogeneous mass distribution in the radial direction. Therefore the separation performance of the column will be improved with a high value of the FQ. As for the effects of the temperature gradient, the relationship between the velocity and the viscosity also plays an important role. Near the wall, the temperature increase causes a decrease of local viscosity and then an increase of the local velocity. If the wall has the same temperature as the eluent at inlet, the tracer near the central part of the column will go further than the tracer near the wall due to the effect of the distributor, leading to the curved tracer profile and peak tailing of the eluted pulse response. Using a suitable higher temperature at the wall, the velocity of the tracer near the wall will be accelerated. In this way the negative effect of the distributor will be counteracted to some extent. Also, through experimental validation, the CFD simulation with FQ100 predicted the optimal temperature difference qualitatively.

This study shows that the CFD simulation is a good tool for understanding the mechanism of the effects of various factors on the performance of the chromatography. Because of the existence of some experiment error, the exact optimal point cannot be absolutely determined. On the other hand, some assumptions were applied to simplify the simulation. Both reasons prevent us from drawing the conclusion that the CFD simulation is capable of making quantitative predictions. However, this work suggests that the CFD is a potential tool for quantitative prediction. The further improvement of experimental technique and software will realise this.

6. Nomenclature

c	Mass fraction of species
C_p	Heat capacity under constant pressure (J/kg, K)
D	Diffusion coefficient (m^2/s)
FQ	Frit quality
h_f, h_s	Enthalpy of the fluid and solid phase, respectively
K	Temperature unit (Kelvin)
L	Length of the fixed bed (m)
P	Pressure (Pa)
Q	Enthalpy (J/kg)
r	Radial coordinate (m)
U	Internal energy (J/kg)
V	Volume (m^3/kg)
T	Temperature (K)
z	Radial coordinate (m)
μ	The first moment, average retention time (s)
σ^2	The second moment, standard deviation
α	Permeability (m^2)
η	Viscosity (P)
ϵ, ϵ_t	External porosity and total porosity, respectively
ρ, ρ_s	Density of fluid and solid phase, respectively (kg/m^3)
λ_f	Fluid heat conductivity (W/m K)
λ_s	Solid heat conductivity (W/m K)

λ_{eff} Effective heat conductivity (W/m K)

References

[1] F.G. Lode, A. Rosenfeld, Q.S. Yuan, T.W. Root, E.N. Lightfoot, J. Chromatogr. A 796 (1998) 3.
[2] T. Yun, G. Guiochon, J. Chromatogr. A 760 (1997) 17.
[3] G. Guiochon, T. Farkas, G-S. Hong, J-H. Koh, M. Sarker, B.J. Stanley, T. Yun, J. Chromatogr. A 762 (1997) 83.
[4] T. Farkas, M.J. Sepaniak, G. Guiochon, AIChE J. 43 (1997) 1964.
[5] M.S. Smith, G. Guiochon, J. Chromatogr. A 827 (1998) 241.
[6] K. Miyabe, G. Guiochon, J. Chromatogr. A 830 (1998) 263.
[7] T. Farkas, M.J. Sepaniak, G. Guiochon, J. Chromatogr. A 740 (1996) 169.
[8] W. Arlt, Y. Beste, M. Lisso, G. Wozny, in: International Symposium on Preparative and Industrial Chromatography and Allied Techniques, Strabourg (Frahlreich) September, 1998.
[9] H. Colin, G. Guiochon, J. Chromatogr. 158 (1978) 183.
[10] W.R. Melander, Cs. Horváth, Chromatographia 18 (1984) 353.
[11] C. Yi, J.L. Fasching, P.R. Brown, J. Chromatogr. 352 (1986) 221.
[12] H.J. Isaaq, M. Jaroniec, J. Liq. Chromatogr. A 675 (1994) 13.
[13] W.S. Hancock, R.C. Chloupek, J.J. Kirkland, L.R. Snyder, J. Chromatogr. A 686 (1994) 31.
[14] K.B. Sentell, N.I. Ryan, A.N. Henderson, Anal. Chim. Acta 307 (1995) 203.
[15] B. Ooms, LC–GC 14 (1996) 306.
[16] O. Dapremont, G.B. Cox, M. Martin, P. Hilaireau, H. Colin, J. Chromatogr. A 796 (1998) 81.
[17] A. Brant, G. Mann, W. Arlt, J. Chromatogr. A 796 (1998) 109.
[18] A. Brandt, G. Mann, W. Arlt, J. Chromatogr. A 796 (1998) 223.
[19] G.W. Colenbrander, Appl. Sci. Res. 48 (1991) 211.
[20] C.K. Harris, D. Roekaerts, F.J.J. Rosendal, F.G.J. Buitendijk, Ph. Daskopoulos, A.J. N Vreenegoor, H. Wang, Chem. Eng. Sci. 51 (1996) 1569.
[21] J.A.M. Kuipers, W.P.M. van Swaaij, Rev. Chem. Eng. 13 (1997) 1.
[22] G. Guiochon, in: Fundamentals of Preparative and Nonlinear Chromatography, Academic Press, Boston, 1994, Chapter VI.
[23] D. Vortmeyer, R. Berninger, AIChE J. 28 (1982) 508.
[24] A. Klein, Thesis for master degree, TU-Berlin, 1999.
[25] Fluent 4.4, in: 2nd ed., User's Guide, Vol. I, Fluent, 1997, Chapter 6.
[26] M. Lisso, G. Wozny, W. Arlt, Y.A. Beste, Chem. Ing. Tech. 72 (2000) 494.
[27] R.H. Perry, D. Green, Perry's Chemical Engineers' Handbook, 6th ed, McGraw-Hill, 1984.